Supplementary Information for

Loss of MPC1 reprograms retinal metabolism to impair visual function

Allison Grenell[a,b] , Yekai Wang[a,b], Michelle Yam[a,b], Aditi Swarup[c], Tanya L. Dilan[a,b], Allison Hauer[a,b], Jonathan D. Linton[d,e], Nancy J. Philp[c], Elizabeth Gregor[a,b], Siyan Zhu[a,b], Quan Shi[a], Joseph Murphy[a,b], Tongju Guan[a,b], Daniel Lohner[a,b], Saravanan Kolandaivelu[a,b], Visvanathan Ramamurthy[a,b], Andrew F. X. Goldberg[f], James B. Hurley[d,e] and Jianhai Du[a,b*]

[a]Department of Ophthalmology, West Virginia University, Morgantown, WV 26506

[b]Department of Biochemistry, West Virginia University, Morgantown, WV 26506

[c]Department of Pathology, Anatomy & Cell Biology, Thomas Jefferson University,

Philadelphia, PA 19107

[d]Department of Biochemistry, University of Washington, Seattle, WA 98109

[e]Department of Ophthalmology, University of Washington, Seattle, WA 98109

[f]Eye Research Institute, Oakland University, Rochester, MI 48309

* Corresponding author: jianhai.du@wvumedicine.org, One Medical Center Dr, PO Box 9193, WVU Eye Institute, Morgantown, WV 26505, (304)-598-6903.

Corresponding author: Jianhai Du
Email:jianhai.du@wvumedicine.org

This PDF file includes:

www.pnas.org/cgi/doi/10.1073/pnas.1812941116

Supplementary Materials and Methods

Animals

MPC1 $^{flox/flox}$ mice in C57 B6 background from Dr. Jared Rutter at University of Utah. These mice were crossed with WT C57 B6/J mice from Jackson lab to breed out the rd8 mutations. To knockout MPC1 in the retina, MPC1 $^{flox/flox}$ mice were crossed with six3 (a pan-retina cre)-Cre mice (1), transferred from Dr. Saravanan Kolandaivelu at West Virginia University. MPC1 $^{flox/flox}$, six3-Cre and MPC1 $^{flox/flox}$/six3-Cre littermates with both sexes were used in this study. We did not observe difference in sexual dimorphism in the MPC KO mice. The sex for each experiment was listed in Table S3. The details for Mouse experiments were performed in accordance with the National Institutes of Health guidelines and the protocol approved by Institutional Animal Care and Use Committee of West Virginia University.

Western blot

Immunoblots were performed as previously reported (2). MPC1 antibody (1:1000) was from Sigma and β-tubulin antibody (1:1000) was from Santa Cruz Technology. The immunoblots were scanned with a Li-Cor Odyssey Blot Imager.

Spectral Domain Optical Coherence Tomography (OCT)

OCT was used to obtain *in vivo* non-invasive cross-sectional images of the retina using the Bioptigen R-series spectral domain ophthalmic imaging system (Bioptigen, Inc., Durham, NC). Mice were anaesthetized through use of an induction chamber with 1.5% isoflurane with 2.5l/min oxygen flow rate at 40°C and then received constant isoflurane during OCT via a nose cone. Both pupils were diluted using a 1:1 mixture of 2.5 % phenylephrine hydrochloride (Paragon Bioteck, Inc., Portland OR) and 1% tropicamide (Sandoz, Inc., Princeton, NJ) for at least 8 min. To prevent corneal desiccation before and during OCT, GenTeal® lubricant eye gel (Alcon, Fort Worth, TX) was applied liberally. Upon dilation and lubrication, mice were positioned on the apparatus and OCT was performed as previously described (Ferguson et. al, 2013).

Transmission electron microscopy (TEM)

Three-month-old FL and their littermate MPC knockout eyes were immersion fixed (2% paraformaldehyde, 2.5% glutaraldehyde in 0.1M sodium cacodylate buffer, pH 7.4) at RT for ~30 minutes. Their anterior segments were removed by dissection, and the eyecups were fixed at RT an additional ~24 hrs. Eyecups were carefully dissected into ~8-12 wedges, which were subsequently washed in 3% sucrose-0.1M sodium cacodylate buffer, pH 7.4, and post-fixed in osmium tetroxide. An ethanol series of increasing concentration was used to dehydrate the tissue. En bloc staining was carried out using 2% uranyl acetate in 70% ethanol step. The tissue was embedded in Polybed 812 (Electron Microscopy Sciences; Hatfield, PA), using proplylene oxide as a transition fluid. Semi-thin sections were cut on a Reichert Ultracut E (Reichert-Jung, Vienna, Austria) ultramicrotome and stained with Toluidine Blue O to assess section orientation. Ultrathin (silver to gold interference) sections from the central retina were mounted on copper grids and post-stained with Uranyless contrasting agent (Electron Microscopy Sciences; Hatfield, PA) and lead citrate. Samples were viewed on a FEI Morgagni 268 TEM at 100

kV accelerating voltage, and imaged using a side-mount Hamamatsu Orca-HR digital camera and AMT Image Capture Engine V601 software (size-calibrated using a grating replica).

Electroretinography (ERG)

FL and MPC knock mice were dark-adapted overnight before ERG using the UTAS Visual Diagnostic System with BigShot Ganzfeld with UBA-4200 amplifier and interface, and EMWIN 9.0.0 software (LKC Technologies, Gaithersburg, MD, USA) as reported. Mice were anesthetized with 1.5% isoflurane with 2.5 l/min oxygen flow rate using an induction chamber and eyes were dilated with a 1:1 mixture of 2.5 % phenylephrine (Paragon) and 1% tropicamide (Sandoz). After ten minutes of dilation, animals were placed on a heated platform (40°C) where they continued to receive a constant flow of isoflurane from a nose cone. A reference electrode was place subcutaneously in the back of the neck (LKC #95-016.) Electrodes made from 0.125 mm silver wire were carefully positioned closely above the cornea with contact being made by GenTeal Tears Lubricant Eye gel (Alcon). All preparation was done under red light. Scotopic recordings were elicited using flashes of LED white light at increasing flash intensities (-32, -24,-16, -12, -4, 0 dB). Responses were averaged at each light intensity. Immediately after scotopic recordings, animals were light adapted for 10 minutes to white background light (30 cds/m^2.) To keep eyes moist, Systane Ultra Lubricant Eye Drops (Alcon) were applied periodically. With continuous background light, photonic response was elicited again with increasing flash intensities (0, 3, 5, 10, 15, 25 dB) again, with LED white light. Values were normalized to the baseline and each eye was evaluated separately to determine the a-wave and b-wave amplitudes.

***In situ* hybridization**

MPC1 RNA in situ hybridization was performed using RNAscope 2.5 HD assay kit (Advanced Cell Diagnostics, Newark, CA) using mouse MPC1 probe (mm-MPC1, Cat. 463291; Advanced Cell Diagnostics)(3). Briefly, fresh frozen sections from one-month-old FL and MPC1 knockout mouse retinas were fixed in 4% pre-chilled paraformaldehyde at 4 °C for 15 min and dehydrated in ethanol series. As per the manufacturer's instructions, the tissue sections were undergone pretreatment, hybridization, amplification, and detection (red assay) steps. Images were captured with a 60× objective (NA 1.2) using Nikon A1R laser scanning confocal microscope.

H&E staining and analysis

After sacrifice, mouse eyes were immediately enucleated and fixed in Excalibur's Z-Fix and processed (Sakura VIP) to paraffin. 4-5 micron sections were cut (AO820) and placed on slides. H&E staining was performed with Gill III hematoxylin (StatLab Medical) and Alcoholic Eosin (StatLab Medical). Images were taken with a Nikon C2 confocal microscope system equipped with a Nikon Ds-Ri2 camera. Large scale images were generated using NIS elements AR 4.50 software with 5% overlap. Outer segment thickness was measured by ImageJ at six different positions of the retina (Fig S2). Nuclei of the outer nuclei layer were counted at each measurement point. The -3 and 3 positions were established by counting 20 nuclei in from the outermost edge. The -1 and 1 positions were defined 20 nuclei away from the optic nerve on the left and right side

respectively. -2 and 2 positions were a point in the middle of the other two measurements. Each measurement was replicated ten nuclei away from the first measurement. For each eye, ten sections were analyzed and the values averaged (20 measurements per position per eye) to get the final thickness and nuclei count.

Cryosection immunohistochemistry (IHC)

After brief fixation of eyes in 4% PFA for 10 min, the cornea was removed and the eye cups were further fixed in 4% PFA for 50 min. After being washed three times in PBS (5 min each), the fixed eye cups were incubated first in 20% sucrose in PBS overnight at 4 ^{o}C and then in 1:1 20% sucrose in PBS and optimal cutting temperature compound (OCT) for 1h, at 30 min the lens was removed. Finally, eye cups were embedded in OCT and frozen in a dry ice/100% ethanol bath. For cryosection IHC, frozen sections were blocked in 10% normal goat serum and incubated with primary antibodies overnight, which was detected through secondary antibody incubation at 1h using Alexa-Fluor 488 or -594 conjugated secondary antibodies (1:1000, Invitrogen).

^{13}C labeled metabolite analysis by GC MS

The metabolites were derivatized by methoxymine hydrochloride followed by N-tertbutyldimethylsilyl-N-methyltrifluoroacetamide (TBDMS) as we described (4, 5). An Agilent 7890B/5977B GC/MS system with an Agilent DB-5MS column (30 m × 0.25 mm × 0.25 μm film) was used for GC separation and analysis of metabolites (5). Ultra–high-purity helium was the carrier gas at a constant flow rate of 1 mL/min. One microliter of sample was injected in split-less mode by the auto sampler. The temperature gradient started at 95 °C with a hold time of 2 min and then increased at a rate of 10 °C/min to 300 °C, where it was held for 6 min. The temperatures were set as follows: inlet 250 °C, transfer line 280 °C, ion source 230 °C, and quadrupole 150 °C. Mass spectra were collected from 80–600 m/z under selective ion monitoring mode. The data was analyzed by Agilent MassHunter Quantitative Analysis Software and natural abundance was corrected by ISOCOR software.

Steady state metabolomics by LC MS/MS

Mouse retinas or RPE/choroid from FL and MPC1 knockout mice at P20 retinas were extracted for metabolites (4, 5). The extracts were analyzed by a Shimadzu LC Nexera X2 UHPLC coupled with a QTRAP 5500 LC MS/MS (AB Sciex). An ACQUITY UPLC UPLC BEH Amide analytic column (2.1 X 50 mm, 1.7 μm, Waters) was used for chromatographic separation. The mobile phase was (A) water with 10 mM ammonium acetate (pH 8.9) and (B) acetonitrile/water (95/5) with 10 mM ammonium acetate (pH 8.2) (All solvents were LC–MS Optima grade from Fisher Scientific). The total run time was 11 mins with a flow rate of 0.5 ml/min with an injection volume of 5 μl. The gradient elution is 95–61% B in 6 min, 61–44% B at 8 min, 61–27% B at 8.2 min, and 27–95% B at 9 min. The column was equilibrated with 95% B at the end of each run. The source and collision gas was N2. The ion source conditions in positive and negative mode were: curtain gas (CUR) = 25 psi, collision gas (CAD) = high, ion spray voltage (IS) = 3800/-3800 volts, temperature (TEM) = 500 °C, ion source gas 1 (GS1) = 50 psi, and ion source gas 2 (GS2) = 40 psi. Each metabolite was tuned with standards for optimal transitions

(Table S1) ^{13}C-nicotinic acid (Toronto Research Chemicals) was used as the internal standard. The extracted MRM peaks were integrated using MultiQuant 3.0.2 software (AB Sciex).

Acylcarnitine measurement by LC MS/MS

Mouse retinas were homogenized in a mixture of cold methanol/chloroform/H_2O (700:200:50). Extracts were dried and analyzed by LC MS/MS as described for steady state metabolite measurement. The parameters for MRM transitions were listed below.

Metabolite	Q1	Q3	Declustering potential	Collision Energy	Retention Time
Stearoyl carnitine	428.5	85.1	70	25	0.34
Myristoyl carnitine	372.4	85.1	66	20	0.44
Decanoyl carnitine	316.3	85.1	64	25	0.44
Hexanoyl carnitine	260.2	85.1	80	25	1.04
2 methylbutyryl carnitine	246.2	85.1	100	43	1.21
Isobutyryl carnitine	232.1	85.1	70	30	1.43
Butyryl carnitine	232.2	85.1	72	30	1.43
Propionyl carnitine	218.1	85.1	60	24	1.61

Mitochondrial oxygen consumption

Four retinas from two mice were quickly dissected using "Winkling" method (5) and mitochondria was isolated with mitochondrial isolation kit (BioVision #K288-50) according to the manual. Mitochondria was added to respiration buffer, consisting of 150 mm KCl, 10 mm KH2PO4, 1 mm MgCl2, pH 7.4 and placed into a respiration chamber, which was connected to an oxygen probe (OXYT1 - Hansatech Instruments, Norfolk, UK). Oxygen respiration was initiated by the addition of pyruvate (1.5 mM) and malate (0.5 mM), ADP (1 mM) and glutamate (1 mM) as described (6). Oxygen consumption were expressed as nanomoles of oxygen consumption rate (OCR) per hour per mg of protein.

Statistics

The significance of differences between means was determined by unpaired two-tailed T tests or analysis of variance with an appropriate post hoc test by Prism 7. $p < 0.05$ was considered to be significant. Metabolomics data was analyzed with Volcano plot ($P<0.05$ and fold change>1.5) using MetaboAnalyst (http://www.metaboanalyst.ca/)

Supplemental Figures

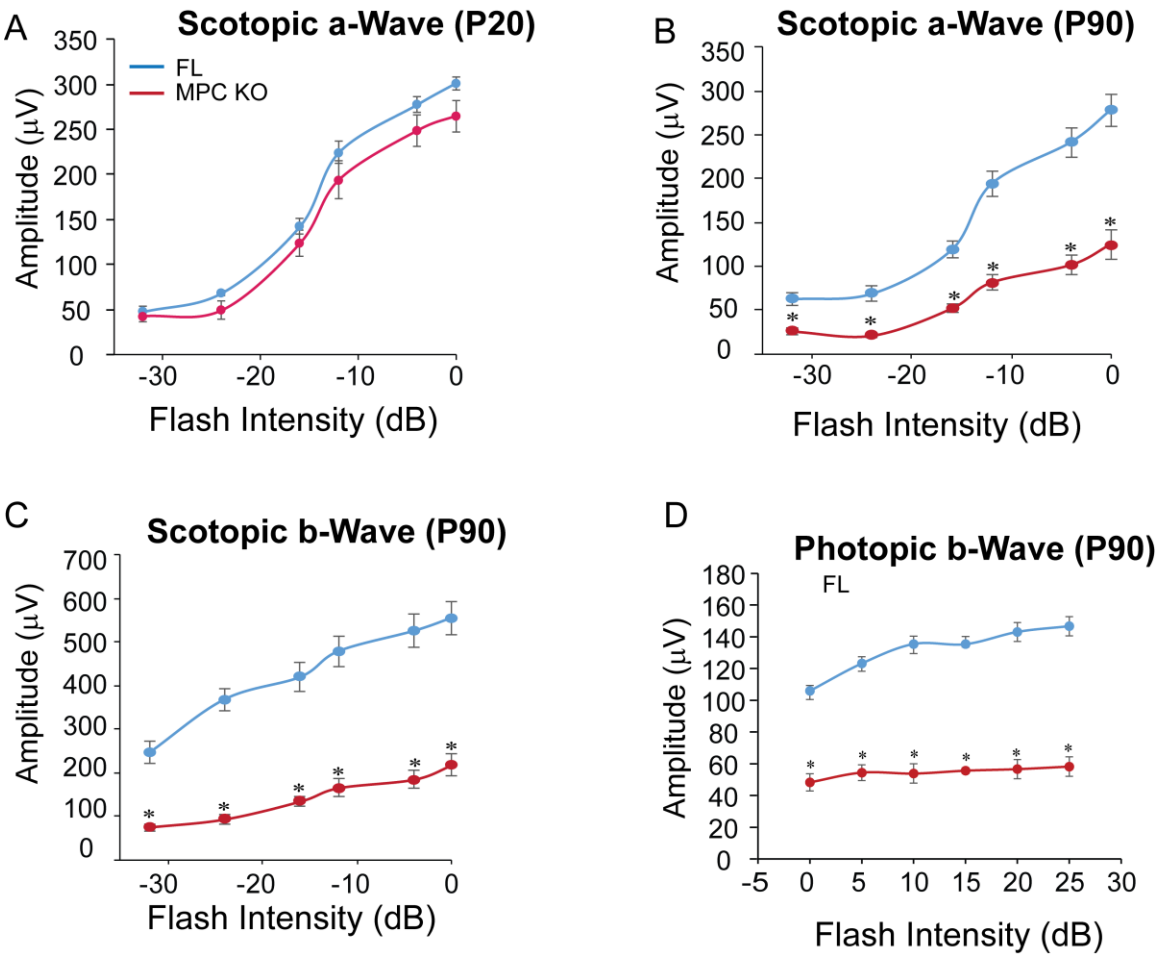

Fig S1. Scotopic and photopic ERGs in MPC KO mice. Scotopic and photopic ERGs were recorded at multiple light intensities in the P20 and P90 MPC KO mice and their littermate controls respectively. Mean ± S.E.; N=6; *P<0.05 vs MPC KO littermates (ANOVA).

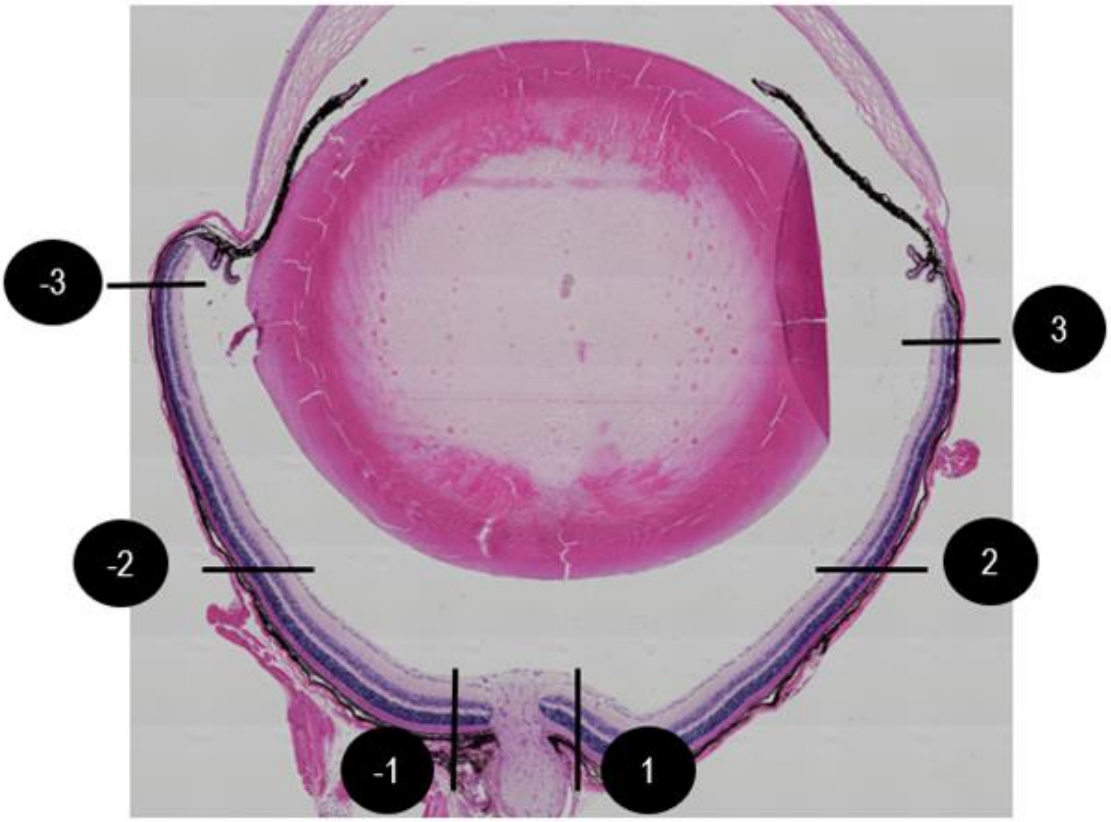

Fig S2. A schematic for H&E data quantitation. For each section, 6 positions (labeled in black lines as -1, -2, -3, 1, 2, 3) chosen to quantify the thickness of retinal layers by image J.

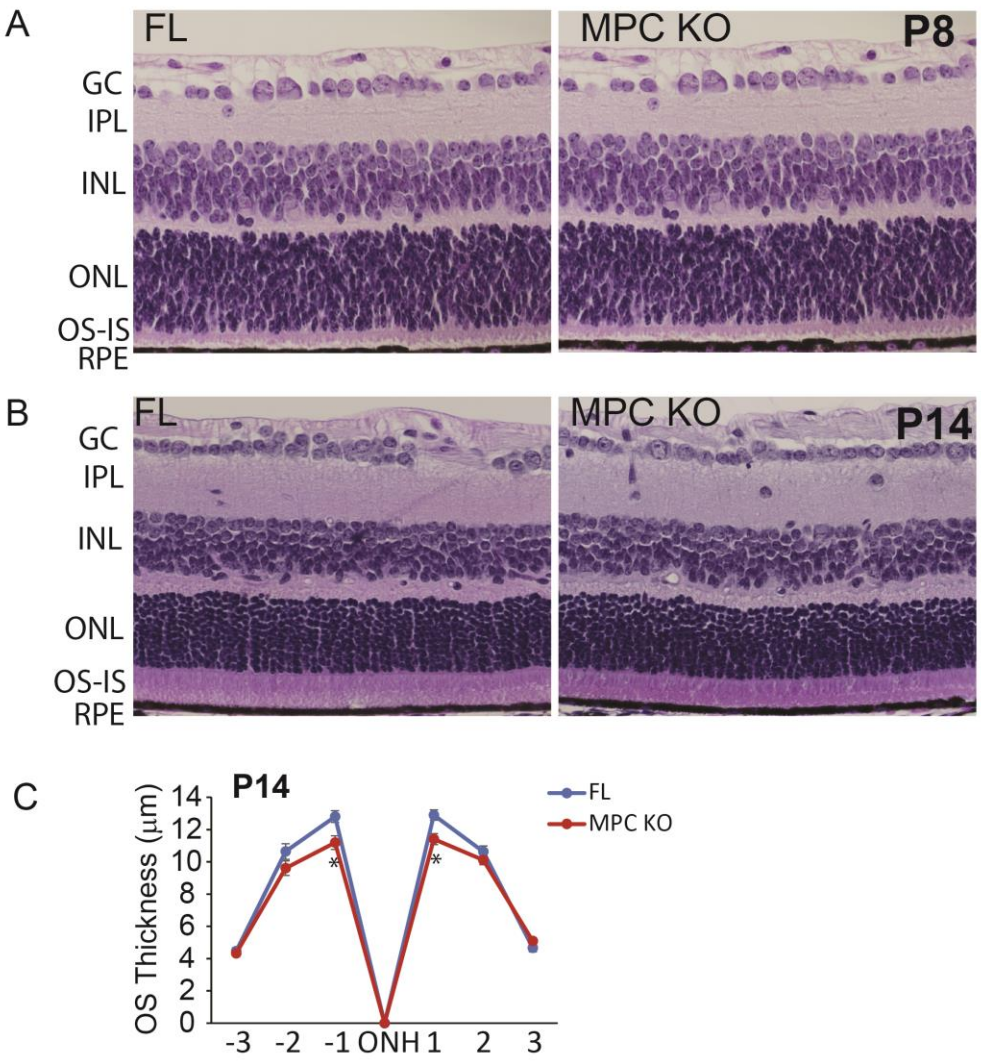

Fig S3. Retinal morphology in the P8 and P14 retinas. (A-B) Eyes from P8 mice and P14 were sectioned for H&E staining. Representative images were at -1 position to the OPN. (C) Quantification of OS thickness in P14 retinas. N=20 from 4 eyes (T test).

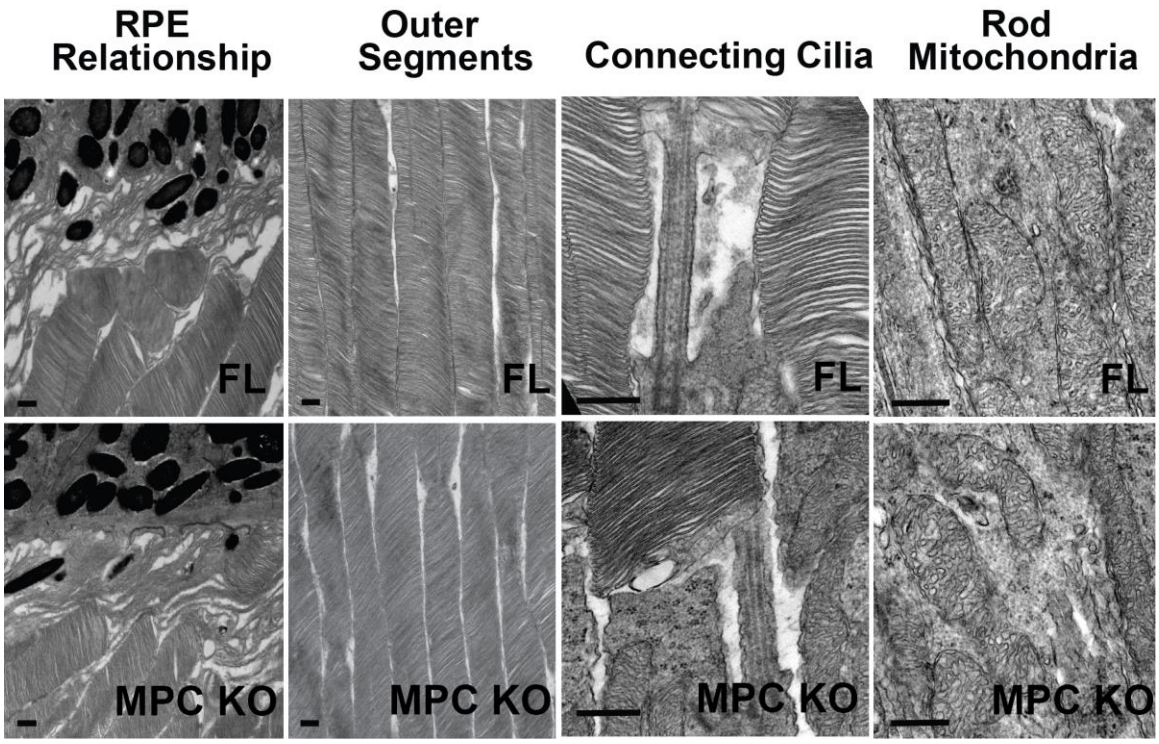

Fig S4. The TEM images of FL and MPC KO retinas. In the P90 MPC KO retinas, the RPE, OS, connecting cilium and mitochondria had normal structure. Scale bar=500 nm. N=4.

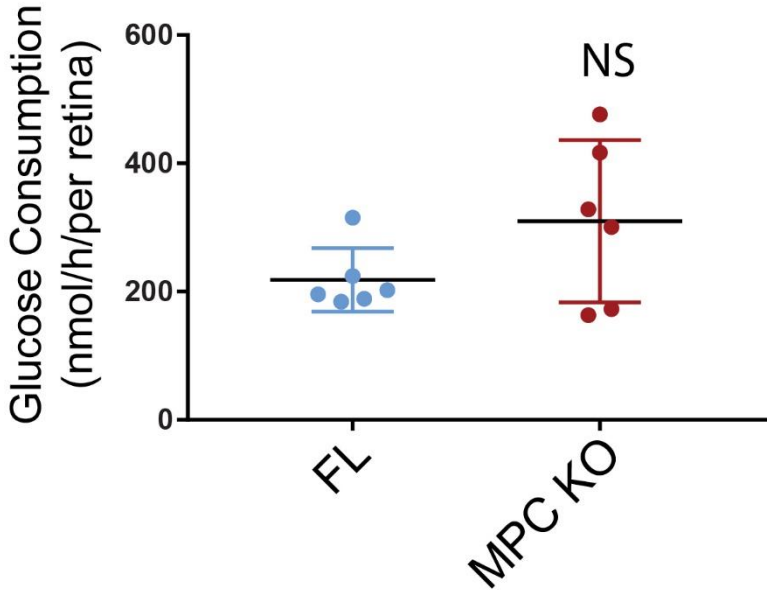

Fig S5. Glucose consumption in the MPC KO retinas. P20 retinas were incubated with 5 mM ^{13}C glucose in KRB (200 μl/per retina) for 1 hour. The ^{13}C glucose consumption was measured by LC MS/MS. NS, no significance (T test). N=6.

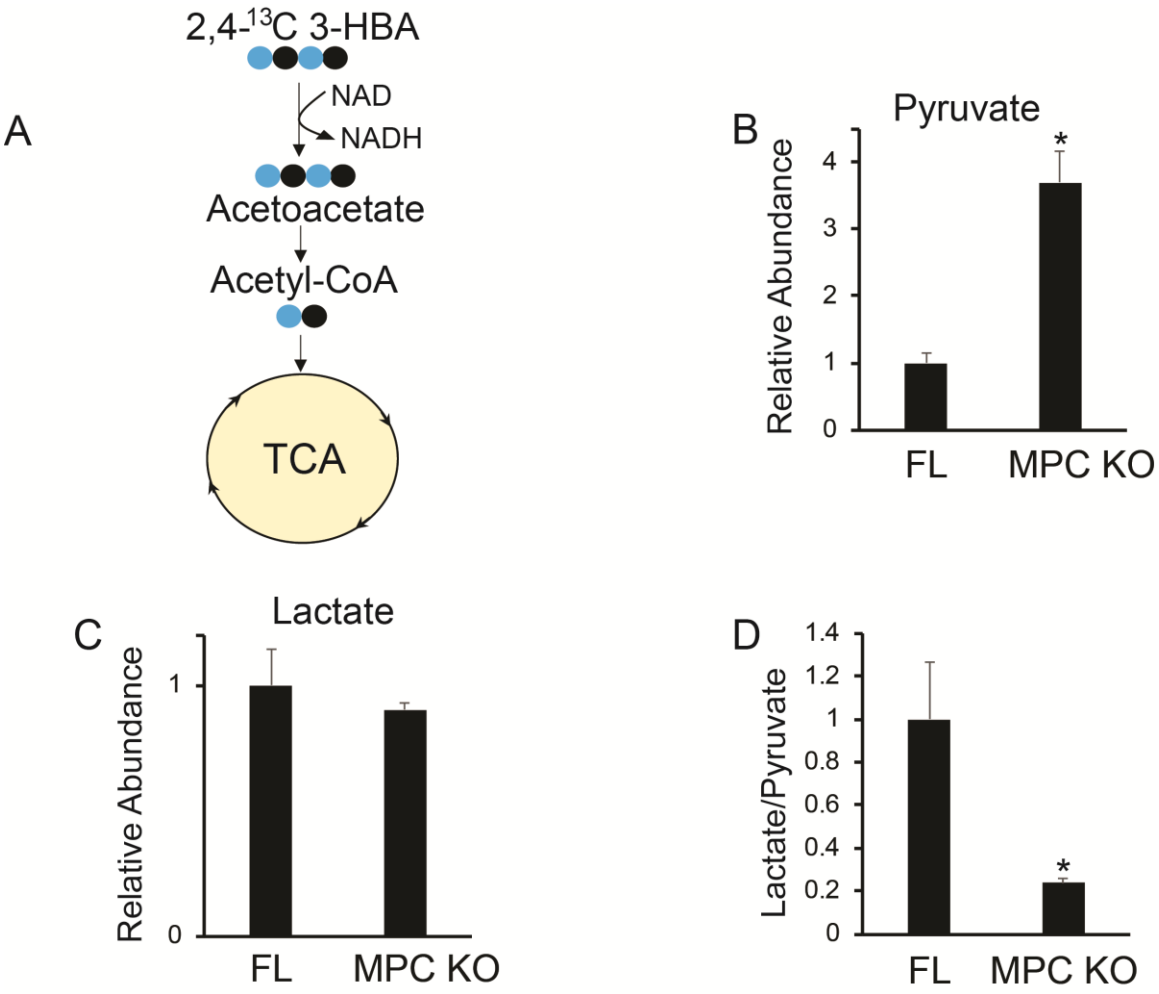

Fig S6. Loss of MPC1 enhances ketone body oxidation and decreases lactate/pyruvate ratio. (A) A schematic for the utilization of ^{13}C 3-HB. (B-C) Mouse retinas at P20 were incubated with 5 mM ^{13}C 3-HB in the presence of 5 mM glucose for 1 hour. (B-D) Unlabeled pyruvate and lactate in the medium were quantified by GC MS. *P<0.05 vs FL (T test), N=6.

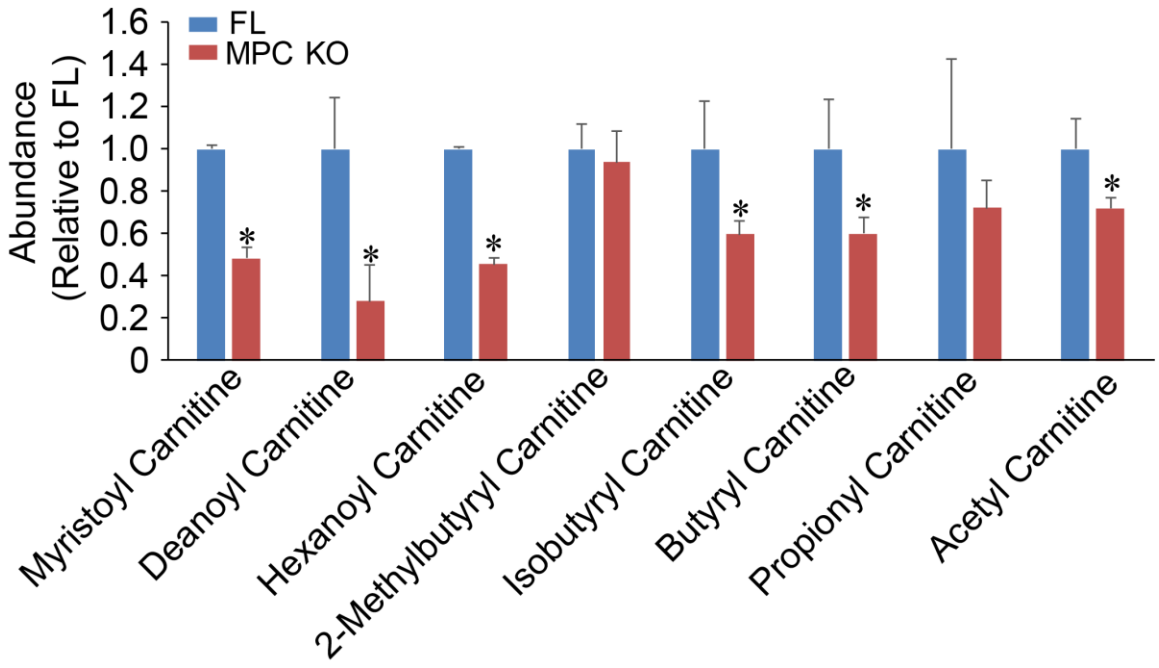

Fig S7. Loss of MPC1 decreases acylcarnitine in the MPC KO retinas. Mouse retinas at P30 were quickly harvested and analyzed for acylcarnitine by LC MS/MS. *P<0.05 vs FL (T test), N=6.

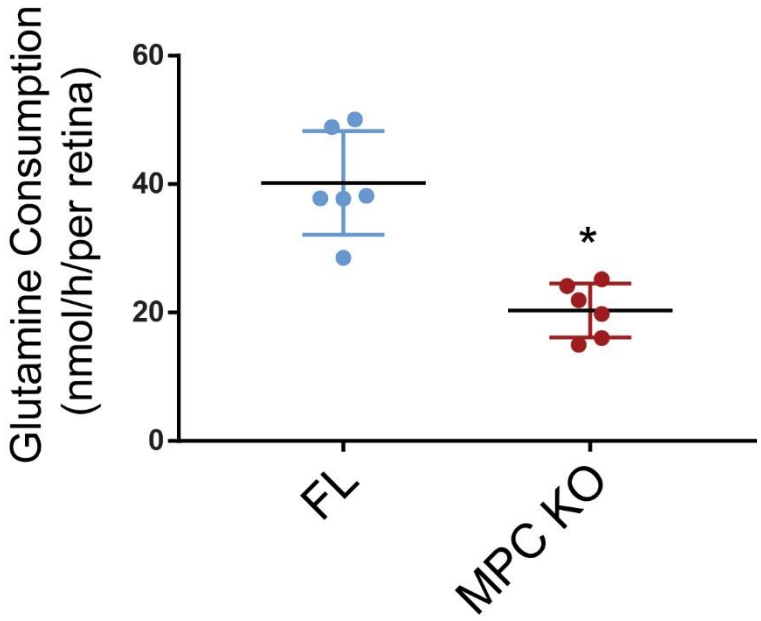

Fig S8. Loss of MPC1 decreased glutamine consumption. Retinas at P20 were incubated with 5 mM unlabeled glucose and 2 mM ^{13}C glutamine for 1 hour. The consumption of ^{13}C glutamine was measured by GC MS. *P<0.05 vs FL (T test), N=6.

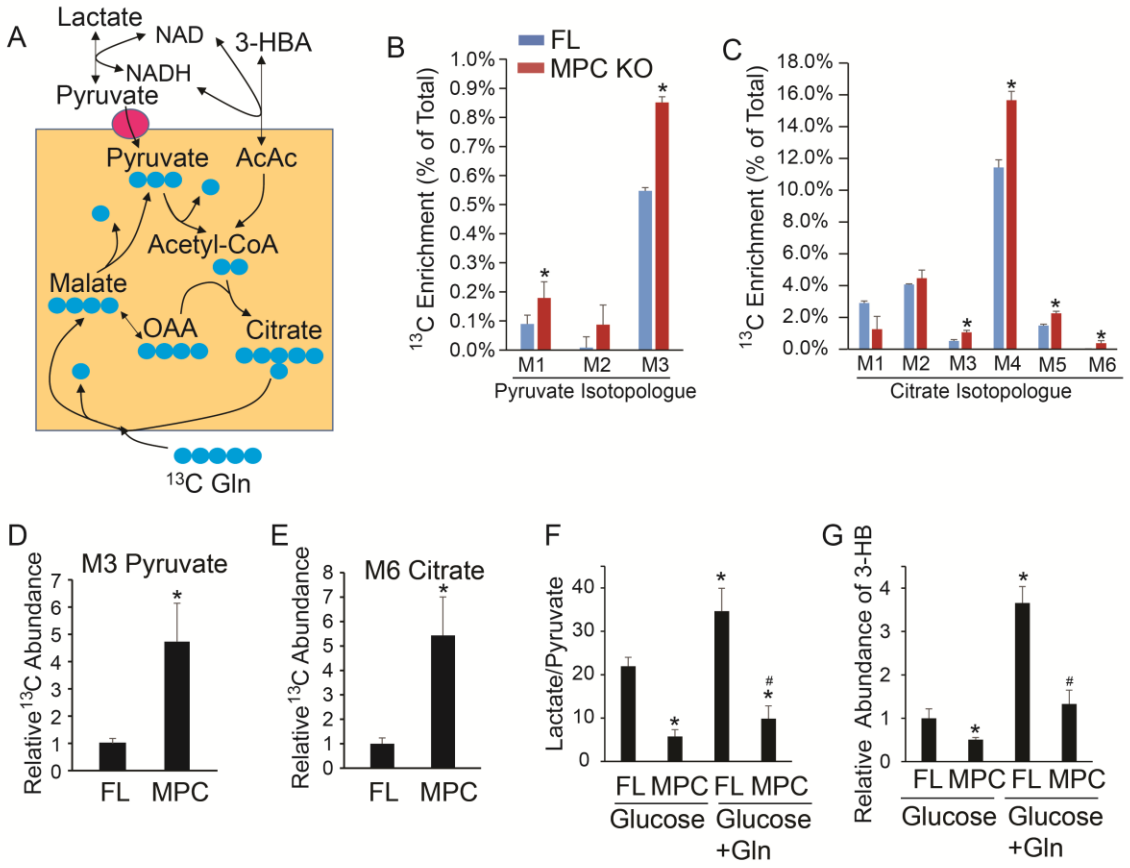

Figure S9. Loss of MPC1 enhances pyruvate production from malic enzyme and disrupts the lactate/pyruvate ratio. (A) A schematic of pyruvate production from 13C-glutamine and regulation cytosolic reducing power. M3 pyruvate could generate from malate through malic enzyme and forms M6 citrate by condensing with M4 OAA. NAD/NADH ratio regulates the balance of both lactate/pyruvate and 3-HBA/Acetoacetate (AcAc). (B-G) Retinas were incubated with 5 mM glucose and 1 mM ^{13}Cglutamine for 1 hour. MPC KO increased the labeled fraction in pyruvate (B) and citrate (C). MPC KO increased the abundance of both M3 pyruvate (D) and M6 citrate (E). Loss of MPC1 decreased lactate/pyruvate ratio from the fuels from both glucose or glucose with glutamine (F). MPC1 KO reduced 3-HB but the reduction was rescued by supplementation with glutamine (G). Data were Mean ± SD. *P<0.05 vs FL (T test) or FL with glucose, #P<0.05 vs FL with both glucose and glutamine (ANOVA). N=3.

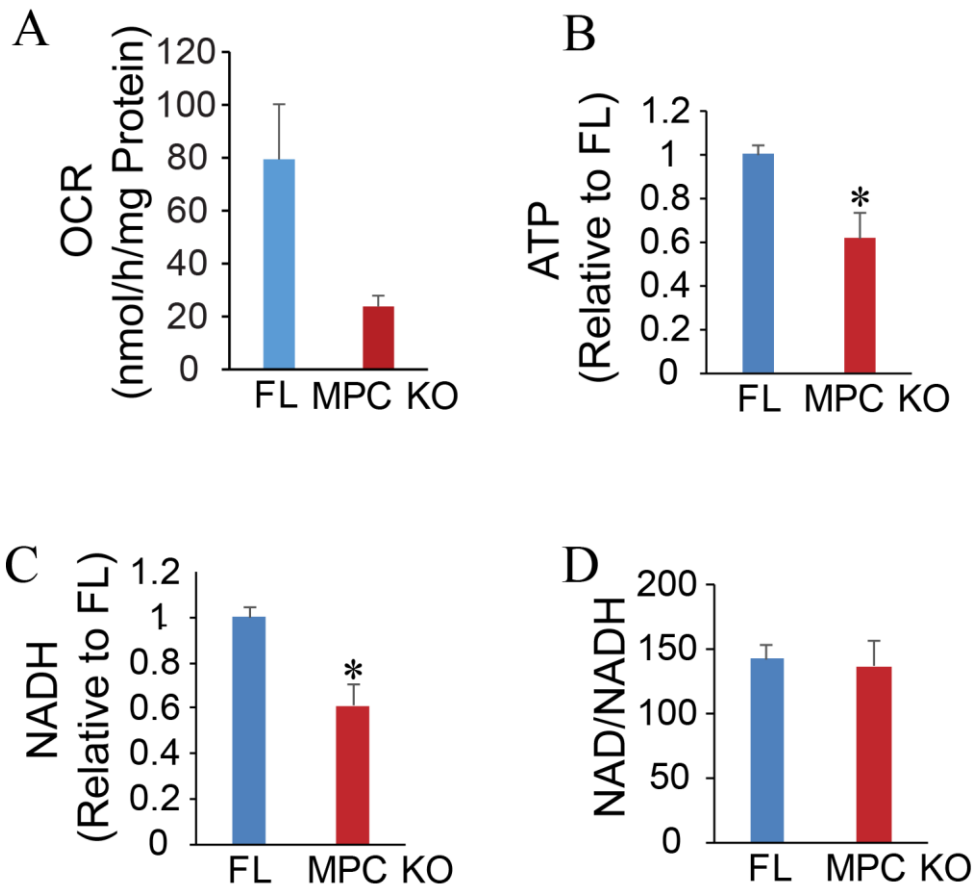

Figure S10. Loss of MPC1 causes mitochondrial dysfunction. (A) MPC KO retina had decreased oxygen consumption rate (OCR). Retinas from two mice at P30 were pooled for mitochondrial isolation and oxygen consumption measurement. *P<0.05 vs FL (T test). N=3. (B-D) ATP, NAD and NADH were measured by LC MS/MS in freshly dissected retinas from P30 mice. The levels of ATP and NADH were the ion intensity abundance relative to FL. NAD/NADH ratio was the ratio of ion intensity. *P<0.05 (T test). N=4.

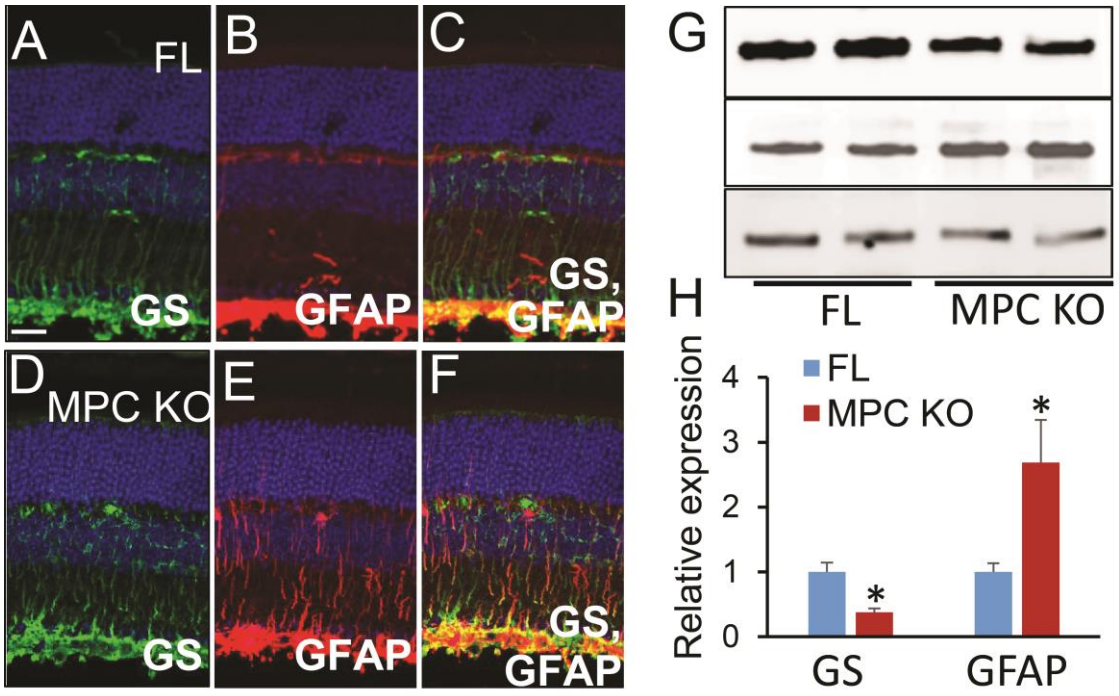

Fig S11. Loss of MPC1 damages and activates Müller glial cells. (A-F) Retinal sections were immunostained with glutamine synthetase (GS), Glial fibrillary acidic protein (GFAP) and overlapping the images between GS and GFAP. Scale bar=20 μm. N=4. (G-H) 10 μg of retinal protein extracts were loaded and immunoblotted with antibodies against GS, GFAP or β-tubulin. (G) was the representative immunoblot and (H) was the quantification of is the quantification of densitometry relative to FL. *P<0.05 vs FL (T Test), N=4.

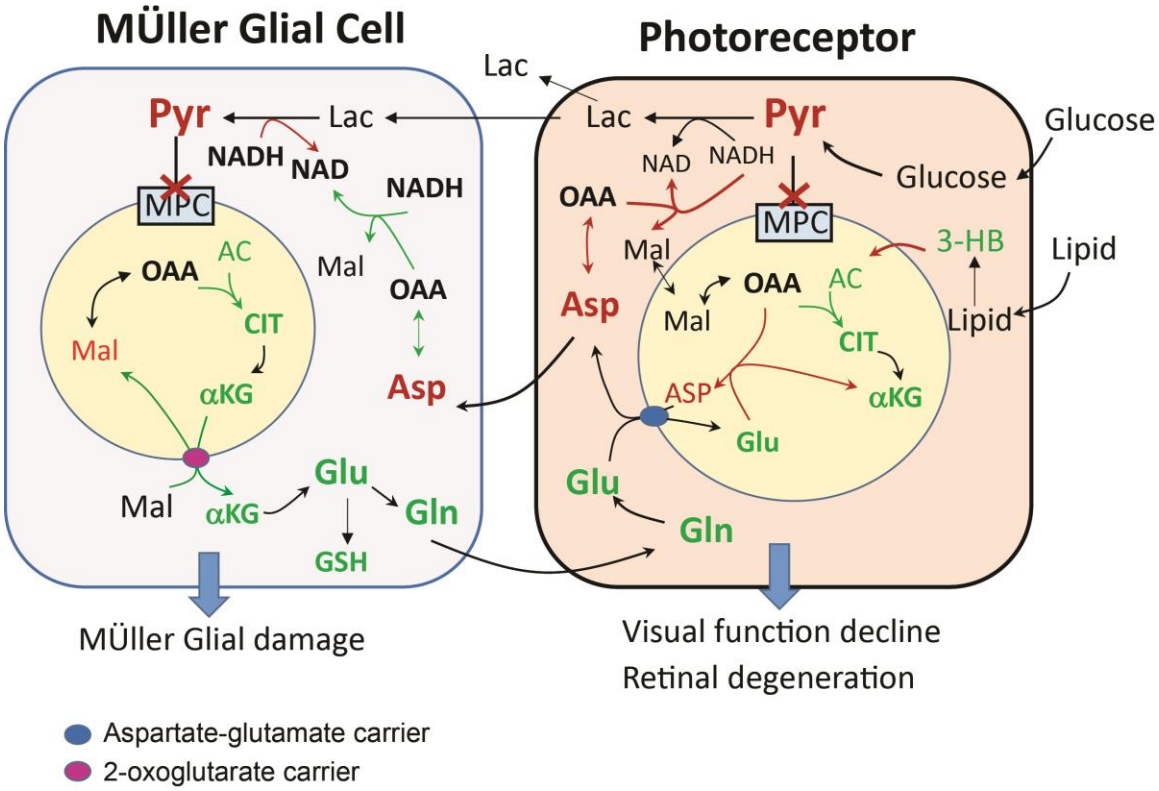

Figure S12. A proposed model for MPC in mouse retinas. Deletion of MPC accumulates glucose-derived pyruvate in the cytosol, which increases cytosolic NADH. This will stimulates malate (Mal) and aspartate (Asp) shuttle to import cytosolic reducing power into mitochondria. Because of the limited availability of mitochondrial acetyl-CoA (AC) from pyruvate, mitochondrial oxaloacetate (OAA) from imported malate are accumulated. OAA is converted into Asp and exported into cytosol. Asp serves as both the carbon and nitrogen source for glutamine synthesis in the glial cells through 2-oxoglutarate carrier. The limited acetyl-CoA in the glial mitochondria accumulates OAA, ASP and Mal, so less Mal from cytosolic Asp is imported into mitochondria and less αKG is exported out. This results in less glutamine biosynthesis from glial cells. The limited acetyl-CoA could also stimulate lipid oxidation and 3-HB utilization. However, this compensation could not fully rescue the MPC deficiency leading to decreased neurotransmitter (glutamate), decreased antioxidant (glutathione) and mitochondrial dysfunction. Subsequently, MPC KO retinas have declined visual function, photoreceptor degeneration and MÜller glial damage**.**

Table S1 List of metabolites and their parameters detected by LC MS

Compound	**Mode (Pos/Neg)**	**Q1 (Da)**	**Q3 (Da)**	**Declustering Potential (Volts)**	**Collision Energy (Volts)**	**Retension time (RT)**
GSH	Neg	306	143.1	-61	-26	3.8
GMP	Neg	362.1	79	-41	-61	4.22
1-Methyladenosine	Pos	282.1	150.1	48	35	1.85
AMP	Neg	346	134	-82	-46	3.76
Salicylate	Neg	137	93	-100	-38	3.13
CoA	Pos	768.1	261	34	47	4.3
IMP	Neg	347	79	-118	-86	4
G3P	Neg	171	79	-74	-28	3.77
Glucose	Neg	179	89	-50	-15	2.07
Glutamine	Pos	147.1	84.1	45	23	3.03
Hippurate	Neg	178	77.1	-61	-23	0.87
Pipecolic acid	Pos	130	84.1	45	12	2.17
Adenosine	Pos	268.1	136	95	38	0.79
N1-Methylnicotinamide	Pos	137	78	110	37	1.63
Guanosine	Neg	282.1	150	-67	-33	1.64
Carnosine	Pos	227.1	110.1	157	32	3.61
Nicotinamide	Pos	123	80	136	20	0.41
Succinyl coenzyme A	Pos	868.1	361.2	45	41	4.97
GSSG	Neg	611	306	-67	-34	5.56
Riboflavin	Pos	377.1	243.1	14	29	1.07
Arginine	Pos	175.1	70.1	45	33	4.28
NMN	Pos	335	123.1	40	25	4.7
Homoserine	Pos	120.1	74	37	16	3.04
Citrulline	Neg	174.1	131.1	-32	-20	3.28
Adenine	Neg	134	107	-92	-25	0.73
Inosine	Neg	267	135	-123	-30	1.1
ophthalmic acid	Pos	290.1	58	139	56	3.66
Heptadecanoic acid	Neg	269.1	135.1	-77	-35	1.05
GDP	Pos	444	152	65	26	5.5
NADP	Pos	744	136	9	78	5.36
Uracil	Neg	111	42	-51	-37	0.53
Choline	Pos	104.1	60.1	95	37	1.51
Azelaic acid	Neg	187	97.1	-73	-25	2.48
Aconitate	Neg	173	85	-37	-18	3.66
3-hydroxybutyric acid	Pos	105.1	23	10	27	2.15
Hypoxanthine	Neg	135	65	-108	-37	0.8
UDP-Glucose	Pos	611	499	40	29	4.59

Citraconic Acid	Neg	129	85	-21	-12	3.63
Xanthine	Neg	151	108	-70	-23	1.1
Acetyl-CoA	Pos	810.1	303.1	116	46	4.17
DUMP	Neg	307	79	-68	-66	3.7
Nicotinamide riboside	Pos	255.1	123	68	18	2.25
5-AminovalericAcid	Pos	118.1	55.1	57	24	3.07
Methylmalonate	Neg	117	73	-58	-14	1.2
Cytidine	Pos	244	112.1	50	30	1.39
3-Aminoisobutyrate	Pos	104.1	58	55	38	1.6
Aminoadipic acid	Neg	145	83	-50	-17	3.14
N-Acetylputrescine	Pos	131.1	114	64	30	1.93
Sarcosine	Pos	90	44	38	17	2.29
Cystathionine	Neg	221.1	79.1	-87	-30	0.57
G6P	Neg	259	79	-46	-62	4.11
4-Hydroxyphenylpyruvate	Neg	179.1	97.1	-40	-17	4.08
NAD	Pos	664	136	27	48	4.33
3-hydroxykynurenine	Neg	223	75	-150	-55	0.3
Fructose 1,6 Biphosphate	Neg	339.1	79	-56	-75	7
ADP	Neg	426	79.1	-65	-84	4.6
UDP	Neg	403	79	-30	-73	4.8
Cadavarine	Pos	103	77	190	25	1.02
Xanthurenic acid	Neg	204	160	-67	-19	1.15
DUMP	Neg	307	79	-68	-66	3.7
Pentothenate	Neg	218.1	88.1	-80	-21	1.74
Creatine	Pos	132.1	90	170	17	2.66
DHAP	Neg	169	79	-38	37	4.11
Pyridoxal-5-P	Neg	246	79.1	-61	-61	3.8
NADH	Neg	664	397	-7	-46	3.91
O-acetyl-l-carnitine	Pos	204.1	85	71	30	1.86
Palmitoyl coenzyme A	Pos	1006.3	499.5	45	53	3.26
Trigonelline	Pos	138	92	60	27	1.81
Spermine	Pos	203.1	129	33	26	1.9
N-oxide	Pos	139	65.1	121	36	0.79
Tyramine	Pos	138	77.1	58	41	1
Carnitine	Pos	163.1	85	100	15	2.6
Glutaric Acid	Neg	131	87	-45	-16	3.41
Betaine	Pos	118.1	58	166	56	1.67
Tryptophan	Pos	205	146	75	35	1.79
FAD	Pos	786.1	136.1	14	46	3.7
cAMP	Neg	328	134	-87	-32	2.28
TMAO	Pos	76	58	137	41	2.05
cGMP	Neg	344	150	-37	-30	2.75
Trans-4-hydroxyproline	Pos	132.1	86	60	17	2.63

Glycerol	Pos	93	51	160	36	0.23
Creatinine	Neg	112	41	-67	-36	0.8
ATP	Pos	507.9	136.1	14	60	5.5
Glycerate	Neg	105	75	-87	-15	1.4
GTP	Neg	521.9	159	-75	-57	5.2
Proline	Pos	116.1	70.1	70	44	2.1
N-acetylglycine	neg	116	74	-37	-14	1.92
Aspartic acid	Pos	134.1	74	50	20	3.49
Maleic acid	neg	115	71	-34	-13	0.54
Nicotinic acid	Neg	122	78	-50	-15	1.31
Uridine	Pos	245	113	23	51	1.4
Pyruvate	Neg	87	43	-44	-11	0.8
Glutamate	Pos	148.1	84.1	51	20	3.3
13C1-Nicotinic acid	Pos	126	79	95	30	1.3

Table S2 Key reagents and resources

REAGENT or RESOURCE	SOURCE	IDENTIFIER
^{13}C tracers		
U-^{13}C glucose	Cambridge Isotope Laboratories	CLM-1396
U-^{13}C glutamine	Sigma-Aldrich	605166
2,4-^{13}C 3-hydroxybutyrate	Sigma-Aldrich	674117
Antibodies		
MPC1	Prestige Antibodies	HPA-045119
β-tubulin	Santa Cruz	sc-55529
GFAP	invitrogen	PA5-16291
Glutamine Synthase	Santa Cruz	sc-74430
Rhodopsin (4D2)		Gift from Dr. Ted Wensel
Na/ K ATPase	Proteintech	22338-1-AP
In Situ Hybridyzation		
mm-MPC1 Probe	Advanced Cell Diagnostics, Newar	463291
RNAscope 2.5 HD assay kit	Advanced Cell Diagnostics, Newar	322360
ERG & OCT		
GenTeal Tears, Severe Lubricant Eye Gel	NDC	0078-0429-47
Systane Ultra, High Percentage Lubricant Eye Drops	NDC	00065-1431-28
Paragon Phenylephrine Hydrochloride Hydrochloride, USP 2.5%	NDC	42702-102-15
Sandoz Tropicamide 1%	NDC	61314-355-02
Mass Spectrometry (LC MS and GC MS)		
Acquity UPLC BEH Amide 1.7 µm Vanguard pre-column 2.1 x 5mm column	Waters	186004799
Acquity UPLC BEH Amide 1.7 µm 2.1 x 50mm column	Waters	186004800
Water, Optima™ LC/MS Grade	Fisher Chemical	7732-18-5
Acetonitrile, Optima™ LC/MS Grade	Fisher Chemical	75-05-8
Ammonium Acetate	Sigma-Aldrich	431311
Ammonium hydroxide 28 - 30% in water ACS	VWR	AC42330-5000
Methoxyamine hydrochloride	Sigma-Aldrich	226904
Pyridine	Sigma-Aldrich	270970

N-tert-Butyldimethylsilyl-N-methyltrifluoroacetamide	Sigma-Aldrich	394882
DB-5ms GC Column, 30 m, 0.25 mm, 0.25 µm,	Agilent Technologies	122-5532
Animals		
MPC1 flox/flox mice	Dr. Jared Rutter	N/A
Six3 CRE mice	Dr. Saravanan Kolandaivelu	N/A
C57 B6/J	Jackson Lab	664

Table S3 List of animals with different sexes used for experiment

Figure	Male (N)	Female (N)
Fig 1	6	7
Fig 2	10	8
Fig 3, Fig S4	4	3
Fig 4	3	3
Fig 5	2	4
Fig 6, Fig S6, Fig S9	7	5
Fig S1	6	6
Fig S3	4	4
Fig S5	4	2
Fig S7	5	1
Fig S8	3	3
Fig S10	8	12
Fig S10	4	4

References

1. Christiansen JR, Kolandaivelu S, Bergo MO, & Ramamurthy V (2011) RAS-converting enzyme 1-mediated endoproteolysis is required for trafficking of rod phosphodiesterase 6 to photoreceptor outer segments. *Proceedings of the National Academy of Sciences of the United States of America* 108(21):8862-8866.
2. Kanow MA, *et al.* (2017) Biochemical adaptations of the retina and retinal pigment epithelium support a metabolic ecosystem in the vertebrate eye. *Elife* 6.
3. Swarup A, *et al.* (2018) Deletion of GLUT1 in mouse lens epithelium leads to cataract formation. *Experimental eye research* 172:45-53.
4. Du J, Linton JD, & Hurley JB (2015) Probing Metabolism in the Intact Retina Using Stable Isotope Tracers. *Methods in enzymology* 561:149-170.
5. Zhu S, *et al.* (2018) Impact of euthanasia, dissection and postmortem delay on metabolic profile in mouse retina and RPE/choroid. *Experimental eye research* 174:113-120.
6. Du J, *et al.* (2013) Inhibition of mitochondrial pyruvate transport by zaprinast causes massive accumulation of aspartate at the expense of glutamate in the retina. *The Journal of biological chemistry* 288(50):36129-36140.